

Contents lists available at ScienceDirect

Petroleum Science

journal homepage: www.keaipublishing.com/en/journals/petroleum-science



Original Paper

Huff-n-puff recovery performance and mechanism analysis of black nanosheets in low-permeability reservoirs based on NMR technology



Si Guo, Hong-Bin Cheng, Hong-Gen Tan, Hong-Yu Li, Jiong Zhang, Ying-Qi Gao, Dao-Yi Zhu *

China University of Petroleum-Beijing at Karamay, Karamay, 834000, Xinjiang, China

ARTICLE INFO

Article history: Received 29 March 2025 Received in revised form 25 May 2025 Accepted 25 May 2025 Available online 26 May 2025

Edited by Yan-Hua Sun

Keywords:
Black nanosheets
Low-permeability reservoirs
Huff-n-puff
Recovery efficiency
Huff-n-puff cycle
Nuclear magnetic resonance

ABSTRACT

Black nanosheets (BNs), as a highly promising fracturing-EOR integrated enhancement material, require further study of their huff-n-puff performance and mechanism. This work characterized nanoscale structure, stability, and interfacial properties of BNs, then evaluated their huff-and-puff performance through NMR-assisted core flooding experiments. The adaptability of BNs in low-permeability reservoirs with different permeabilities, as well as the effect of huff-n-puff cycles on their oil recovery performance, were analyzed. Results show that anionic modified BNs maintained nanoscale flake structure with enhanced electrostatic repulsion. The BNs with an extremely low concentration of 0.002 wt% exhibited excellent emulsification and stabilization effects on crude oil and wettability alteration of the rock surface. Compared with injection water, BNs had excellent huff-n-puff oil recovery effects, reaching 22.1% original oil in place (OOIP) after the first huff-n-puff cycle. BNs had good adaptability in low-permeability cores (i.e., 0.1×10^{-3} to 10×10^{-3} µm²). Increasing the huff-n-puff cycle significantly improved the oil recovery effect of BNs, and the optimal performance was at 4 cycles. As the huff-n-puff cycle increased from 3 to 4, the ability of BNs to "automatic oil-seeking" in micropores became more prominent. This paper also innovatively combined core nuclear magnetic resonance (NMR) T_2 analysis, nuclear magnetic imaging analysis, and longitudinal T_2 signal analysis along the core (i.e., along the core injection length). It can not only more accurately quantify the huff-n-puff recovery effect of low-permeability cores but also quantitatively analyze the penetration depth and microscopic huff-n-puff mechanism of BNs from a microscopic perspective. These findings are helpful for the selection of nanomaterials and mechanism analysis in the design of integrated fracturing-flooding schemes and processes

© 2025 The Authors. Publishing services by Elsevier B.V. on behalf of KeAi Communications Co. Ltd. This is an open access article under the CC BY-NC-ND license (http://creativecommons.org/licenses/by-nc-nd/4.0/).

1. Introduction

As an important part of global oil and gas resources, low-permeability reservoirs have always been one of the major challenges faced by the petroleum industry due to their high development difficulty and low recovery efficiency (Wang P. et al., 2024; Zhu et al., 2024b). The traditional water flooding development method has limited oil recovery effectiveness in low-permeability reservoirs. This is mainly because the pore structure of low-permeability reservoirs is complex, with low permeability and high capillary force, which makes it difficult for injection water to

development of low-permeability reservoirs due to its unique physical and chemical properties and the action mechanism at the microscale (Xu et al., 2024; Zhou B. et al., 2022). Nanoparticles have a high specific surface area, good dispersibility, and interfacial activity, which can effectively reduce the oil–water interfacial tension and improve the wettability of rocks, thereby enhancing the fluidity of crude oil (Almahfood and Bai, 2018; Wu et al., 2024). Therefore, the nanoparticle displacement has great application potential in low-permeability reservoirs and has

become an important research direction for enhancing oil recovery

effectively displace crude oil (Fan H. et al., 2024; Qin et al., 2024;

Zhu et al., 2024; Zuo et al., 2024). In recent years, as an emerg-

ing method for enhancing oil recovery, the nanoparticle dis-

placement has gradually become a research hotspot in the

E-mail address: chutaoi@163.com (D.-Y. Zhu).

(Davoodi et al., 2022).

^{*} Corresponding author.

The black nanosheet (abbreviated as BN), as a emerging nanoparticle displacement material, has demonstrated significant advantages in enhancing crude oil recovery efficiency in recent years (Qu et al., 2021; Raj et al., 2019; Zhu et al., 2024a, 2024b). The BN is primarily composed of carbon-based materials and possesses excellent adsorption, dispersibility, and interfacial activity, which can effectively improve the interaction at the oil-water interface (Feng et al., 2022), Zhu et al. (2024a) modified the BN with anionic surfactants such as cetyltrimethylammonium bromide and urea, enabling it to exhibit good dispersion stability in aqueous solutions. Studies have shown that the BN can significantly enhance the fluidity of crude oil through mechanisms such as reducing oil-water interfacial tension, altering rock wettability, and enhancing emulsification during the oil-displacement process (Geng et al., 2024; Zhu et al., 2023). Additionally, the BN exhibits excellent thermal and chemical stability, allowing it to maintain its oil-displacement performance under complex reservoir conditions (Zhu et al., 2024a, 2024c). Currently, the BN oil-displacement system has been field-tested in multiple oilfields, achieving favorable application results (Qu et al., 2022). However, further indepth research is still needed on the microscopic mechanisms of the BN oil-displacement system and its adaptability in lowpermeability reservoirs.

The huff-n-puff recovery technology, as a cyclic injectionsoaking-production method, has shown promising application prospects in low-permeability reservoirs (Mo et al., 2024). By periodically injecting oil-displacement agents and extracting crude oil, the huff-n-puff technology can effectively improve the development efficiency of low-permeability reservoirs (Fan O. et al., 2024; He et al., 2024). In recent years, nano-assisted huffn-puff or fracturing extraction technology has gradually become a research hotspot (Al-Muntasheri et al., 2017; Bai et al., 2023; Quintero et al., 2018). During the huff-n-puff or fracturing process, nanoparticles can enhance the fluidity of crude oil through mechanisms such as improving rock wettability, reducing oil-water interfacial tension, and enhancing emulsification, thereby increasing the recovery efficiency (Zhang et al., 2024; Zhao et al., 2024). Studies have shown that nano-assisted huff-n-puff or fracturing extraction technology can significantly improve the recovery efficiency of low-permeability reservoirs (Wang Q. et al., 2024; Yekeen et al., 2019; Zhou M. et al., 2022). However, its mechanisms and adaptability still require further exploration. Xu et al. (2023) incorporated BNs into the fracturing fluid system, increasing the recovery efficiency during the spontaneous imbibition stage to 35.43%. Currently, research on nano-assisted fracturing or huff-n-puff extraction technology mainly focuses on the dispersion stability, emulsification performance, and wettability improvement of nanoparticles (Xu et al., 2023; Zhou B. et al., 2022). However, further in-depth research is still needed on the adaptability of nanoparticles in low-permeability reservoirs during the huff-n-puff process and their impact on recovery efficiency.

This study aimed to conduct an in-depth investigation into the huff-n-puff performance of BNs in low-permeability reservoirs and their underlying mechanisms. First, the microscopic morphology of BNs was observed using transmission electron microscopy, and the dispersion stability of BN aqueous solutions was analyzed through zeta potential and multiple light scattering. The emulsification performance of BNs with crude oil and their ability to modify the solid–liquid–liquid three-phase contact angle were evaluated. Second, based on nuclear magnetic resonance (NMR) technology, the huff-n-puff effects of BNs were compared with those of formation water (as the blank control group), and the adaptability of BNs in core samples with different permeabilities in low-permeability reservoirs was analyzed. Finally, the influence of the huff-n-puff cycle on the recovery efficiency of BNs was

investigated. Through the above research, this study could provide a theoretical basis and technical support for the application of the BNs, offering new ideas and methods to enhance the recovery efficiency in low-permeability reservoirs.

2. Experimental materials and methods

2.1. Experimental materials

Anionic modified black nanosheets (BNs) were obtained through hydrothermal reaction and anionic modification using cetyltrimethylammonium bromide, urea, and conventional BNs, following the method described by Zhu et al. (2024a). This method endowed the BNs with improved dispersion stability and oil-displacement performance. The modified BNs had a particle size of approximately 70 nm \times 400 nm and dispersed uniformly in formation water or injection water. Heavy water, provided by Sigma with a deuterium (D) content of 99.95%, was used for NMR analysis. Crude oil from the Mahu Oilfield (viscosity of 7.5 mPa·s) and formation water (for solution preparation) were provided by the Xinjiang Oilfield. The total salinity of the formation water was 20,512 mg/L, with ion compositions of 5362 mg/L Na⁺ & K⁺, 2377 mg/L Ca²⁺, 49 mg/L SO $_4^2$ -, 12,032 mg/L Cl⁻, and 691 mg/L HCO $_3$ -. The water type was identified as CaCl₂.

The core samples used in the experiments were low-permeability or ultra-low-permeability artificial outcrop sand-stone cores with a length of 7 cm and a diameter of 2.5 cm. The permeability range of the cores was (0.1–10) \times $10^{-3}~\mu m^2$. The specific specifications and parameters of the core samples are listed in Table 1, and they were primarily used for huff-n-puff experiments.

2.2. Preparation method of BN solution

Based on previous research (Zhu et al., 2024a), this study adopted the anionic BNs at an optimized concentration (0.002 wt %) as the foundation for analyzing its adaptability to huff-n-puff cycles and operational protocols. A certain amount of BN powder was added to a uniformly stirred aqueous solution (e.g., formation water or heavy water) and stirred at 600 rpm for 10 min. The mixture was then sonicated for 5 min at 40 kHz and 300 W using an ultrasonic homogenizer to obtain the final BN solution. The BN solutions prepared with formation water (H_2O) were primarily used for interfacial property tests, while those prepared with heavy water (D_2O) were employed in huff-n-puff experiments to minimize analytical errors.

2.3. Microstructural characterization of BNs

To elucidate the microstructural properties of BNs and analyze its mechanistic roles (e.g., migration and plugging capabilities) during huff-n-puff processes in low-permeability reservoirs, field-emission transmission electron microscopy (TEM, Tecnai G2 F20, Thermo Fisher Scientific, USA) was utilized. Samples were prepared via standard carbon film deposition, and imaging was conducted at an accelerating voltage of 200 kV to observe low-magnification morphology.

2.4. Zeta potential measurement of BN solutions

Zeta potential analysis was performed to evaluate the electrical charge of nanoparticles, providing insights into their dispersion stability and long-term stability in solution. A dynamic light scattering (DLS) instrument (Malvern Zetasizer Pro, Malvern Panalytical, UK) was used to measure the surface zeta potential of

Table 1Basic physical properties of core samples for huff-n-puff experiments.

Core No.	Length, cm	Diameter, cm	Gas permeability, $10^{-3} \ \mu m^2$	Porosity, %	Water permeability, $10^{-3} \mu m^2$
10-3	7.052	2.528	10.0	17.98	3.85
5-3	7.065	2.521	5.0	17.84	2.05
5-1	7.056	2.521	5.0	18.05	1.65
1-3	7.046	2.514	1.0	14.43	0.27
0.5-3	7.029	2.485	0.5	13.20	0.06
0.1-3	7.085	2.526	0.1	12.01	0.01

BN solutions at ambient temperature and unadjusted pH (i.e., original sample conditions).

2.5. Multispectral light dispersion stability analysis of BN solutions

Multispectral light dispersion analysis was recently introduced to assess the suspension stability of particulate solutions by detecting transmission light variations at different sample heights, thereby evaluating solution stratification. Compared to the particle charge analysis in Section 2.4, this method offered more intuitive insights into dispersion stability. A Turbiscan Lab stability analyzer (Formulaction, France) was employed. BN solutions were loaded into cuvettes with a fixed sample height of 45 ± 0.5 mm and scanned for 6 h. Stability was analyzed based on changes in the scanning profiles.

2.6. Evaluation of BN emulsification performance

The BN solution prepared in Section 2.2 was mixed with crude oil at a volume ratio of 9:1 (total volume: 10 mL) in test tubes. After homogenizing via 200 reciprocating cycles in a vortex mixer, the mixtures were then aged in a 65 °C constant-temperature oven. Emulsification behavior was monitored at intervals to evaluate performance of BNs under various subsurface conditions (e.g., near-wellbore, distant reservoir regions, and prolonged exposure).

2.7. Evaluation method for huff-n-puff performance using BNs

Fig. 1 illustrates the experimental setup and flowchart for the BN huff-n-puff tests. The apparatus consisted of a constant-pressure/rate injection pump, liquid containers, a core holder, two hand pumps, a backpressure regulator, valves, pressure gauges, and a fluid collection system. The experimental procedure was as follows.

- (1) The BN solution prepared with heavy water (Section 2.2) was loaded into designated liquid containers. Crude oil and heavy water (as the control group) were separately loaded into corresponding containers.
- (2) The pre-weighed core sample was placed into the core holder. The attached hand pump was used to pressurize the annular space to 30 MPa. The core holder was heated to 65 °C using heating tapes.
- (3) Oil Saturation: The core holder outlet was connected to a vacuum pump and evacuated for 5 h. All valves were closed, after which the valves between the crude oil container and the core holder were opened. The core was saturated with oil at a flow rate of 0.02 mL/min.
- (4) "Huff" phase: The crude oil outlet valve was closed, and the BN solution (or heavy water, as the control group) outlet valve was opened. The solution was injected at a constant pressure of 25 MPa for 10 min to equilibrate the system.
- (5) "Soaking" phase: All valves were closed, and the system was maintained at 65 °C (simulating reservoir temperature) under pressurized conditions ("soaking") for 12 h.
- (6) "Puff" phase: The backpressure regulator was pressurized to 15 MPa using the hand pump. The valve between the regulator and the core holder inlet was opened to slowly release fluids ("puff" phase). The produced fluids were collected and measured using a fluid sampling device, after which the core sample was weighed.
- (7) For multi-cycle huff-n-puff experiments, steps (4) to (6) were repeated multiple times.

Table 2 outlines the experimental design for the BN huff-n-puff tests, including comparisons of different agents (BN vs. heavy water), evaluations in cores with varying permeability, and multicycle adaptability assessments.

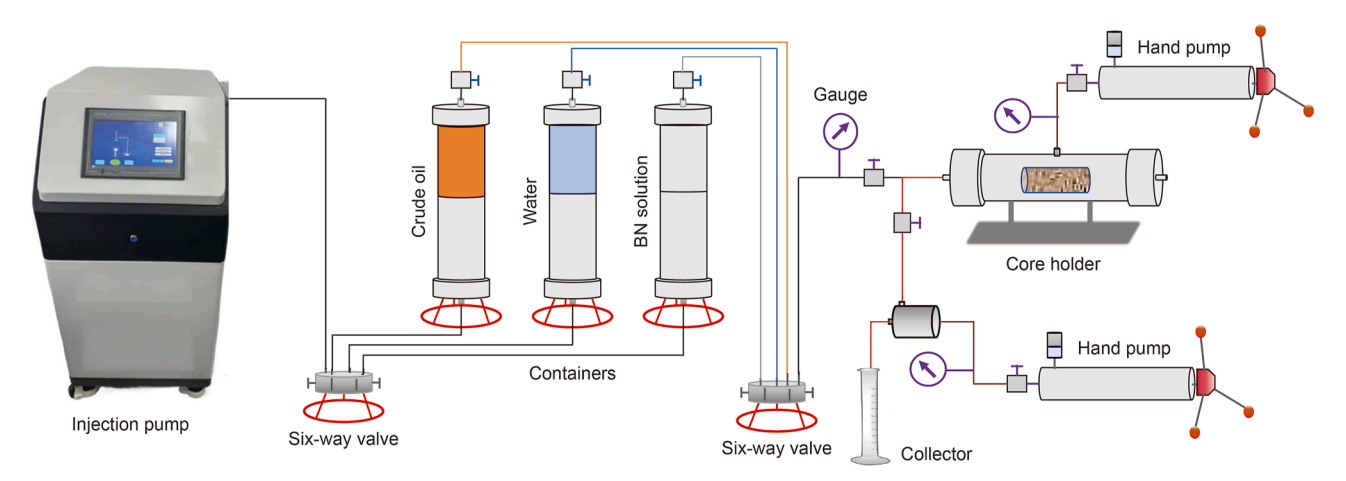


Fig. 1. Experimental apparatus and flowchart for BN huff-n-puff oil recovery tests.

Table 2 Experimental design for BN huff-n-puff tests.

No.	Core No.	Gas permeability, $10^{-3}\ \mu m^2$	Huff-n-puff agent	Huff-n-puff cycle(s)	Remarks
1	5-1	5.0	Heavy water	1	Agent comparison
2	5-3	5.0	BN (heavy water)	5	Cycle comparison
3	10-3	10.0	BN (heavy water)	1	Permeability comparison
4	1-3	1.0	BN (heavy water)	1	
5	0.5-3	0.5	BN (heavy water)	1	
6	0.1-3	0.1	BN (heavy water)	1	

2.8. Nuclear magnetic resonance imaging and T₂ signal analysis

2.8.1. NMR imaging analysis

During the BN huff-n-puff experiments described in Section 2.7, NMR technology was employed to detect T_2 signals during the huff-n-puff process. This approach was adopted to reduce uncertainties caused by significant measurement errors in low-permeability core samples (where oil production during huff-n-puff was typically very small). Since deuterium oxide (D_2O) did not generate NMR signals, NMR technology enabled real-time analysis of residual oil distribution during the huff-n-puff process to investigate its mechanisms.

A high-temperature and high-pressure NMR assisted flooding system (SPEC-RC035, Beijing Spec Technology Co., Ltd.) was used for imaging analysis of the core sample during huff-n-puff operations. The CORE-T1-128T module was selected for analysis, with parameters as follows: repetition time (TR) was 500, number of excitations (NEX) was 8, receiver gain (RG) was 5, slice thickness (THK) was 100.0 mm/10 mm, and matrix size (MAT) was 128 \times 128 pixels.

2.8.2. NMR T₂ analysis

NMR T_2 analysis was conducted to quantify residual oil in macropores and micropores within the core sample, which provided insights into the microscopic mechanisms of BNs (or other agents like D_2O) entering pore spaces during huff-n-puff. A full-core signal scan was performed during T_2 analysis. Dwell time (DW) was 2 μ s, number of echo sampling points was 1, number of acquired echoes was 4096, scan repetitions was 64, signal gain (RG) was 20 db, and waiting time was 3000 ms.

2.8.3. Longitudinal T₂ signal analysis along the core

To analyze the spatial distribution of T_2 signals along the length of the core sample during huff-n-puff, longitudinal T_2 signal analysis along the core distance were measured. Experimental parameters matched those in Section 2.8.1 for NMR imaging. The scan direction was set to start from the core inlet and terminate at the core outlet.

3. Results and discussion

3.1. Interfacial and oil-water performance analysis of BNs

3.1.1. Microstructure of BNs

To evaluate the compatibility of BNs with pore sizes in low-permeability reservoirs, the microstructure of BN was analyzed using the TEM method described in Section 2.3, as shown in Fig. 2.

As shown in Fig. 2, the BN exhibited a two-dimensional sheet-like morphology at the nanoscale, with an average diameter of ~700 nm and thickness of ~5 nm. Fig. 2(a) and (b) display top views of the nanosheets, showing a loosely stacked configuration. Fig. 2 (c) highlights the ultrathin nanosheet thickness and nanoscale dimensions, which are critical for analyzing injection pressure and oil recovery performance during the huff-n-puff process.

3.1.2. Zeta potential and dispersion stability of BNs

Zeta potential analysis is an important method for evaluating the dispersion stability of nanoparticles in solution. According to the method in Section 2.4, the zeta potential of 0.002 wt% BN in aqueous solution (formation water) was measured, and the results are shown in Fig. 3(a). Multiple light scattering analysis further quantified the dispersion stability of BNs in aqueous solution, and the experimental results are shown in Fig. 3(b).

From Fig. 3(a), it can be seen that the BN exhibited good dispersibility in aqueous solution. Since the zeta potential of the BN was -26.9 mV, its absolute value was large, indicating that the surface of BNs presented a strong negative charge. Therefore, it could generate electrostatic repulsion between particles in the solution. This helped maintain the stability of the BN solution during pumping and propagation.

Fig. 3(b) confirms that the BN solution remained stable after 6 h of aging at reservoir temperature (65 $^{\circ}$ C). When tested at 65 $^{\circ}$ C for 6 h, the change rate of transmitted light was very small, demonstrating its good dispersion stability. This corresponded to the charge analysis in Fig. 3(a), as the BN surface carried a strong negative charge, resulting in strong repulsion between particles, thus ensuring stability. Additionally, due to the low concentration of BNs, its light transmittance was close to 90%.

In addition, no visible particle floating or sedimentation was observed at the top or bottom of the test vial. Minor localized reductions in transmittance occurred but were negligible. These findings indicated that BN was suitable for field applications as a stable nanoparticle recovery agent.

3.1.3. Emulsification performance of BN solution with crude oil

Nanoparticles have the inherent ability to spontaneously accumulate at the oil–water interface, thereby influencing the interfacial activity between oil and water. Using the crude oil emulsification evaluation method described in Section 2.6, the emulsification performance between the 0.002 wt% BN solution and crude oil was investigated and compared with the aqueous solution without BNs (i.e., formation water). The experimental results are shown in Fig. 4. The experiment was conducted at a temperature of 65 °C with an aging time of 5 h.

As can be clearly seen from Fig. 4, BNs exhibited strong crude oil emulsification performance and a certain degree of emulsion stability. Fig. 4(a) shows the emulsification performance of formation water and Mahu crude oil without the addition of BNs. It can be observed that a certain degree of emulsification occurred between the formation water and crude oil, with the emulsion volume being approximately 1.9 mL. Compared to the initial crude oil volume of 1 mL, this nearly doubled. However, after adding 0.002 wt% BNs, the emulsion volume significantly increased to approximately 8 mL. This is mainly because BNs could rapidly accumulate at the oil–water interface and disperse under mixing conditions. When the aging time gradually increased to 10 min, the emulsion stability weakened slightly, but the emulsion volume remained much larger than that of the formation water. Additionally, as the aging time further increased, the emulsion

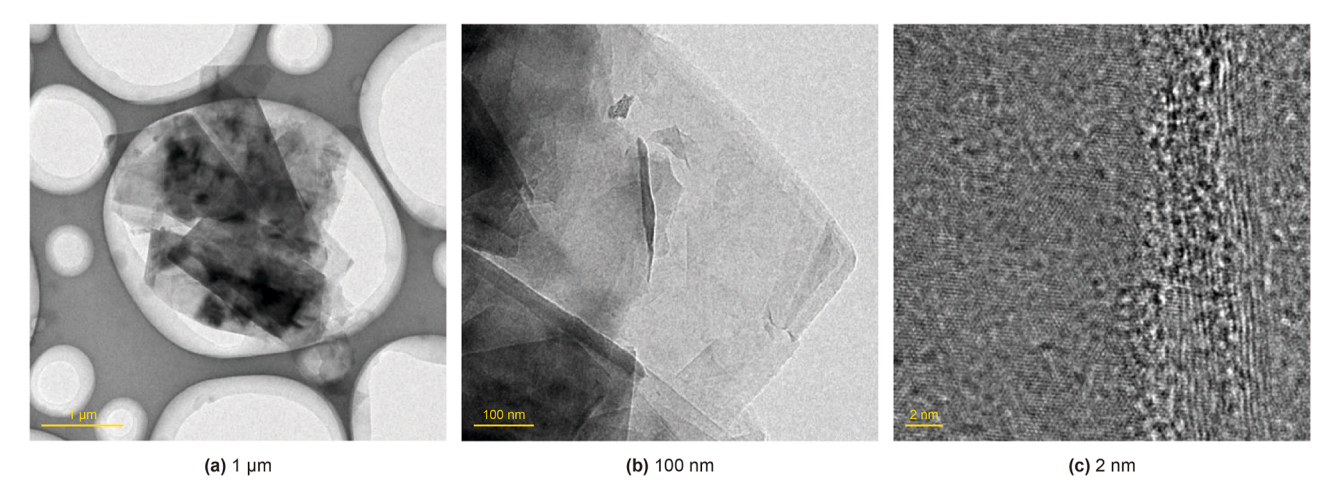


Fig. 2. Microstructure of BNs (TEM images at different resolution scales).

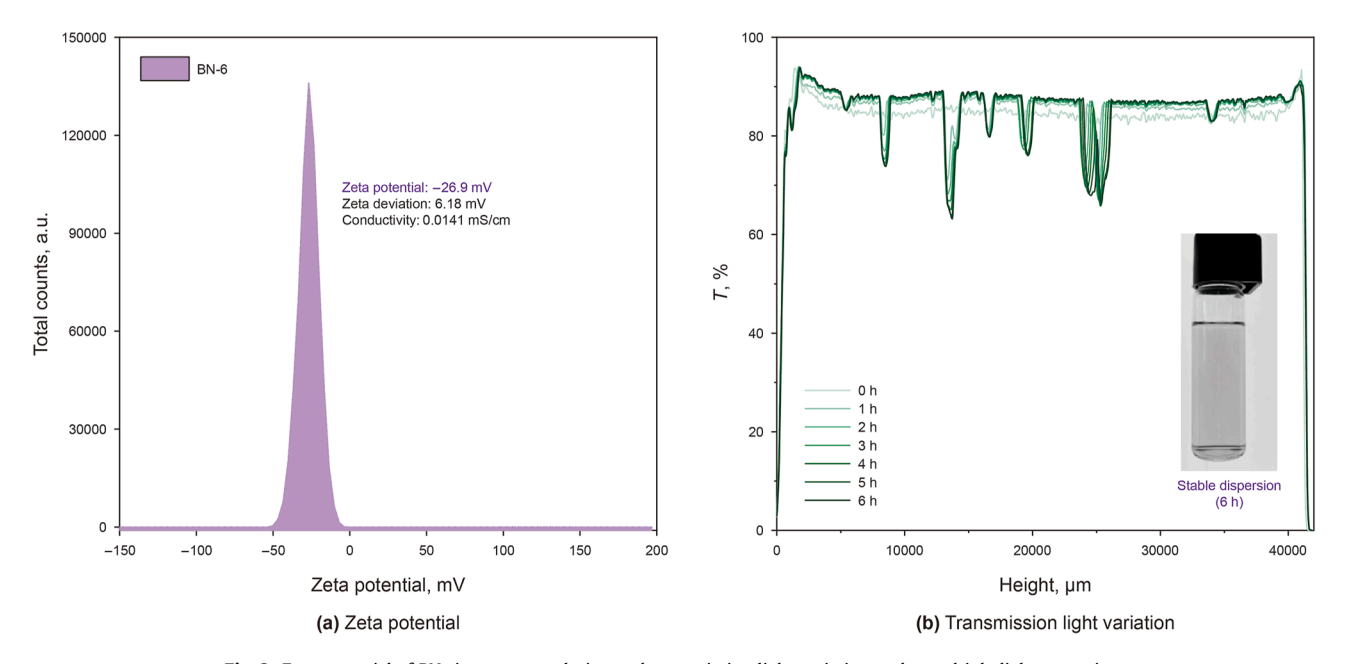


Fig. 3. Zeta potential of BNs in aqueous solution and transmission light variation under multiple light scattering.

remained relatively stable, with the final emulsion volume being approximately 3.1 mL, demonstrating good emulsion stability.

Fig. 5 presents the solid-liquid (oil)-liquid (water) three-phase contact angle measured on the core surface using a contact angle measuring instrument (DSA25S, KRÜSS, Germany). The upper part of the image corresponded to the rock slice, the middle black droplet represented crude oil, and the lower transparent part was the aqueous solution to be tested. The core sample was oilsaturated, and as shown in Fig. 5(a), the oil droplet spread on the surface of the oil-saturated core sample. After adding BNs, the three-phase contact angle was separated by BNs, meaning the addition of BNs increased the wedge pressure, making it easier for the oil droplet to detach from the core sample surface and "scrape" out the crude oil. In summary, it could be concluded that the BN solution significantly improved the interfacial activity between the solution and crude oil. These analytical results would also facilitate the subsequent mechanistic analysis of BN huff-n-puff process.

3.2. Production performance and mechanism analysis of BN huff-n-puff

3.2.1. Comparison of huff-n-puff performance with different agents in 5 \times 10 $^{-3}$ μm^2 core samples

In the development of low-permeability reservoirs, due to the extremely low matrix permeability, methods such as repeated fracturing followed by flowback or huff-n-puff are typically employed for production. The principle of these two methods is similar: injecting fluid into the formation at a certain pressure through production wells and then flowing back for production. To analyze the effectiveness of BN in huff-n-puff process in low-permeability reservoirs, the experimental evaluation method for BN huff-n-puff oil recovery in Section 2.7 was used. A comparison was made between water and BN solution as huff-n-puff agent in terms of recovery efficiency and pressure changes during huff in low-permeability core samples with the permeability of 5 \times $10^{-3}~\mu\text{m}^2$, as shown in Table 3. Heavy water (D₂O, with no NMR signal) was used as the huff-n-puff agent to facilitate subsequent



Fig. 4. Comparison of crude oil emulsification performance with/without BN in formation water. BE denotes before emulsification; JE stands for just emulsification; the other time points represent the aging time after emulsification.



Fig. 5. Three-phase contact angle changes between formation water, crude oil, and rock with/without BN.

Table 3 First-cycle huff-n-puff performance of different agents in $5 \times 10^{-3} \, \mu m^2$ core samples.

Core No.	Gas permeability, $10^{-3} \ \mu m^2$	Huff-n-puff agent	"Huff" pressure change, MPa	Recovery efficiency, %
5-1	5.0	Heavy water	-0.13	48.4
5-3	5.0	BN (in heavy water)	1.35	54.6

NMR analysis of the core samples.

As shown in Table 3, the BN solution demonstrated better huffn-puff performance compared to water in low-permeability core samples with a permeability of 5 \times 10⁻³ μm^2 . The recovery efficiency of the BN solution reached 54.6% original oil in place (OOIP), which was 6.2 percentage points higher than water (48.4% OOIP). This improvement was attributed to BN's superior oil-water interfacial properties (e.g., emulsification and wettability alteration) and its ability to penetrate deeper into the formation to displace crude oil (validated later via NMR). Additionally, the pressure of the BN solution increased by 1.35 MPa during soaking, while that of water decreased by 0.13 MPa. This was mainly because, during huff, the BN had strong interfacial activity (i.e., interfacial tension) (Zhu et al., 2024a), allowing it to enter the core sample more effectively under high-pressure injection (this will be verified and analyzed in subsequent NMR experiments). During soaking, the injected fluid expanded due to continuous heating, leading to a significant increase in pressure. This indirectly indicated that BNs could more easily enter the formation. Therefore, the pressure increase during soaking did not imply that the pressure would increase when BNs were injected into an actual reservoir. Since the outlet of the experimental core sample was sealed with an iron core, this study only considered the huff-n-puff effect. In actual oilfield huff-n-puff process, the reservoir was approximately infinite, and the pressure during constant-rate injection of the BN could be lower than that of water (Zhu et al., 2025).

Furthermore, the dynamic pressure changes during the huff-npuff process are shown in Fig. 6. The pressure during soaking first increased and then decreased. This may be because, in the early soaking stage, the thermal expansion volume of the huff-n-puff agent exceeded the volume entering the pores, leading to a rapid increase in pressure. Since the BN had stronger oil–water interfacial activity and lower capillary resistance (Zhu et al., 2024a), it should enter the core sample more effectively during huff (in this experiment, a constant pressure of 25 MPa was maintained for 10 min). This will be demonstrated and analyzed in subsequent NMR results. When the volume of the huff-n-puff agent gradually stabilized, the agent diffused through the matrix pores toward the outlet under the combined action of soaking pressure and capillary force, and the local high pressure at the inlet gradually propagated

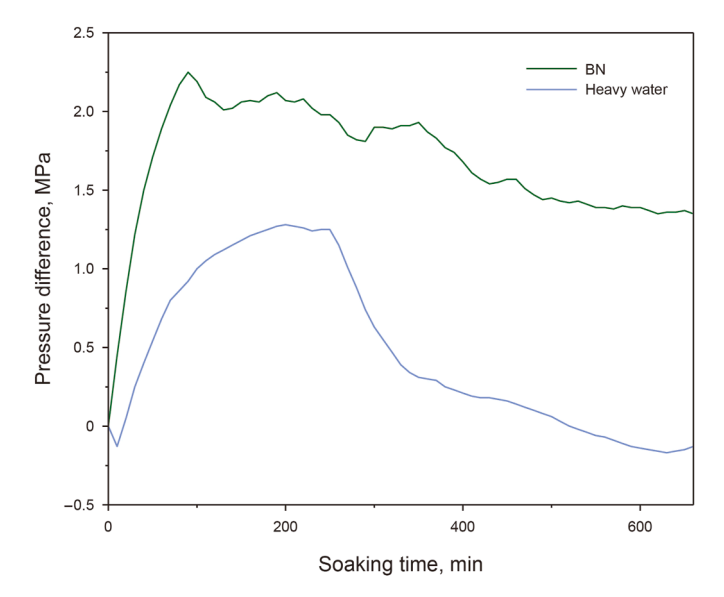


Fig. 6. Comparison of pressure dynamics during soaking after the first huff for different agents in $5 \times 10^{-3} \mu m^2$ core samples.

to low-pressure areas, showing a gradual decrease in pressure gradient. Due to the strong interfacial activity between the BN solution and crude oil, BNs spontaneously accumulated at the oil-water interface (Feng et al., 2022). As a result, its pressure exhibited persistent fluctuations (i.e., continuous recovery). In contrast, no significant pressure fluctuations were observed for heavy water during soaking.

In addition, in actual oilfield applications, the water injection pressure of hydraulic fracturing-flooding technology is usually greater than the formation fracture pressure, which is used to replenish the energy deficit in old wells or improve water injectivity in low-permeability reservoirs. During the soaking phase, pressure rapidly dissipates through the fracture network, and finally, the crude oil in the matrix pores could displace into microfractures under the action of imbibition.

3.2.2. T_2 signal comparison of different agents in $5\times 10^{-3}~\mu\text{m}^2$ core samples

To compare the oil mobilization in pores of different sizes within a $5 \times 10^{-3} \ \mu m^2$ low-permeability core sample under different huff-n-puff agents, the core NMR T_2 analysis method (Section 2.8.2) was used. The changes in NMR T_2 signals at different huff-n-puff stages for both agents are shown in Fig. 7. Since the huff-n-puff agents were prepared with heavy water (D₂O), the NMR T_2 signals reflected only the residual oil within the core.

From Fig. 7, the overall NMR T_2 signal amplitude after BN huffn-puff was lower than that after water huff-n-puff. Specifically, the right peak signal amplitude decreased from 128 to 91 a.u. after BN treatment, which was lower than the 95 a.u. peak after water treatment. Since a relaxation time > 10 ms represents macropores, the signal amplitude reduction after BN huff-n-puff occurred in both macropores and micropores compared to water.

To quantitatively analyze the recovery efficiency of BN versus water in different pore sizes, the cumulative NMR T_2 signal amplitude was calculated to determine the recovery efficiency, as shown in Fig. 8. In macropores ($T_2 > 10$ ms), BNs achieved a recovery efficiency of 24.30%, 3.25 percentage points higher than water (21.05%). In micropores ($T_2 < 10$ ms), the BN recovery efficiency was 17.42%, 0.51 percentage points higher than water (16.91%). Additionally, the overall recovery efficiency for BN huffn-puff was 22.1%, indicating better oil recovery capability. These results were consistent with the weight-based calculations in Table 3 but showed significant numerical differences. Since NMR

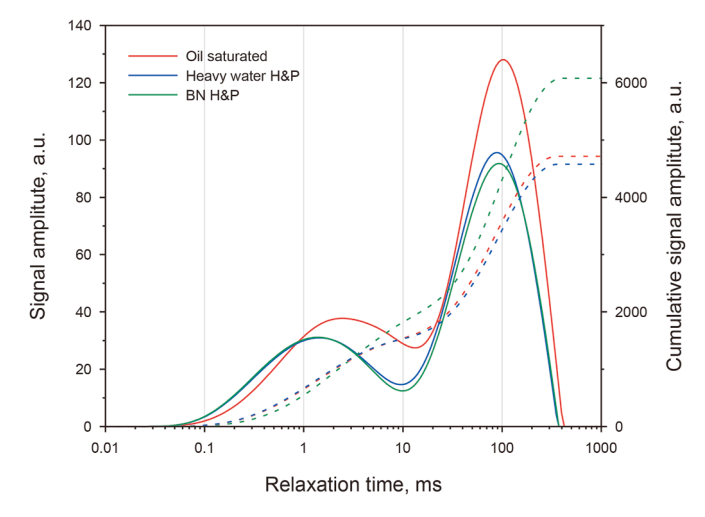


Fig. 7. T_2 signal comparison before and after the first huff-n-puff (H&P) cycle for different agents in $5 \times 10^{-3} \mu m^2$ core samples.

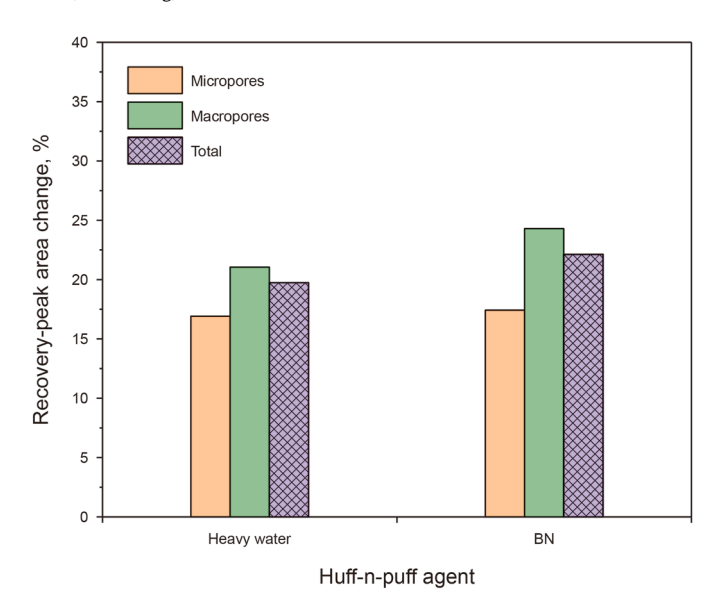


Fig. 8. Peak area comparison of T_2 signals before and after the first huff-n-puff cycle.

directly monitored oil signal changes without interference from heavy water entering dead volumes under high pressure, it provided more accurate recovery efficiency measurements, especially for low-permeability cores with minimal oil production.

3.2.3. NMR imaging comparison of different agents in 5 \times 10 $^{-3}\,\mu\text{m}^2$ core samples

To more intuitively observe oil mobilization in different pore sizes during the huff-n-puff process, the NMR imaging analysis method (Section 2.8.1) was used. NMR images of the low-permeability core samples ($5 \times 10^{-3} \mu m^2$) before and after huff-n-puff with BN and water were obtained, as shown in Fig. 9.

From Fig. 9, it can be directly observed that the grayscale intensity of the NMR images decreased after both BN and water huffn-puff compared to the oil-saturated state. Notably, the grayscale reduction was more pronounced at the right end of the core after BN treatment than after water treatment. This may be because, in the later stages of huff-n-puff, as the pressure field gradually stabilized, BN could more effectively alter rock wettability compared to water. Consequently, under lower pressure gradients, capillary forces helped detach and displace oil from the pore surfaces in the

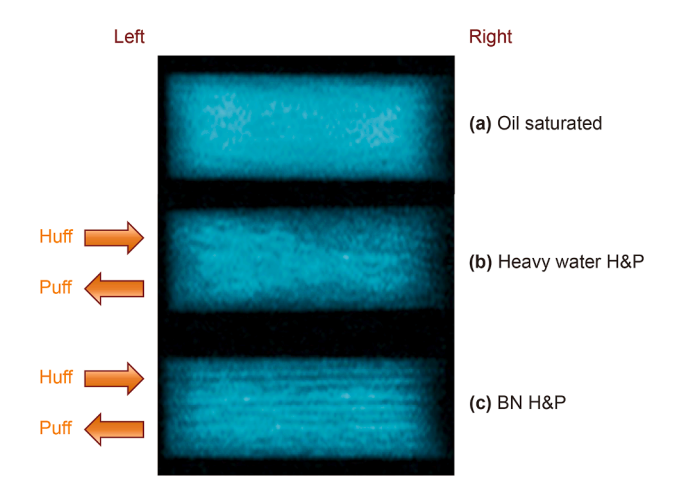


Fig. 9. NMR imaging comparison of different huff-n-puff agents in $5\times 10^{-3}~\mu\text{m}^2$ core samples.

distal core regions. Thus, BN solution could penetrate deeper into the reservoir and displace more oil than water, indicating that BN as a huff-n-puff agent can migrate farther.

3.2.4. Longitudinal T_2 signal comparison of different agents in $5\times 10^{-3}~\mu m^2$ core samples

Section 3.2.3 provided a visual observation of pore mobilization after huff-n-puff with different huff-n-puff agents. However, due to the low imaging resolution, the penetration distances of modified BN and water were not quantified. Fig. 10 shows the changes in longitudinal T_2 signal before and after huff-n-puff with BN solution and water in $5 \times 10^{-3} \ \mu m^2$ core samples.

From Fig. 10, within the 30–100 mm test range, the core exhibited clear signal amplitude, matching its actual length. The scan direction was set from left (huff-n-puff end) to right. Both BN and heavy water significantly entered the left end of the core, leading to a noticeable signal reduction. Additionally, the signal amplitude of BN decreased slightly faster than that of heavy water, mainly because BN could more easily enter pores in the core. Notably, the signal amplitude at the right end of the core showed significant differences, likely due to variations between core samples. Therefore, the analysis should combine NMR imaging results and longitudinal T_2 signal projection for accuracy. To minimize errors, the same core sample was used in subsequent experiments of huff-n-puff cycles.

3.3. Analysis of BN huff-n-puff processes

The oil recovery performance of BN in huff-n-puff applications for low-permeability reservoirs was significantly affected by permeability. Additionally, its recovery efficiency varied greatly across different huff-n-puff cycles. Based on previous studies of BN's interfacial properties and huff-n-puff performance, this section further investigated its adaptability under different permeability conditions and its recovery efficiency across multiple cycles. The findings provided experimental support for optimizing oilfield huff-n-puff operations.

3.3.1. Permeability adaptability of BNs for huff-n-puff process Artificial sandstone core samples with permeabilities of 0.1 \times 10^{-3} to $10\times10^{-3}~\mu m^2$ were used. The huff pressure was 25 MPa,

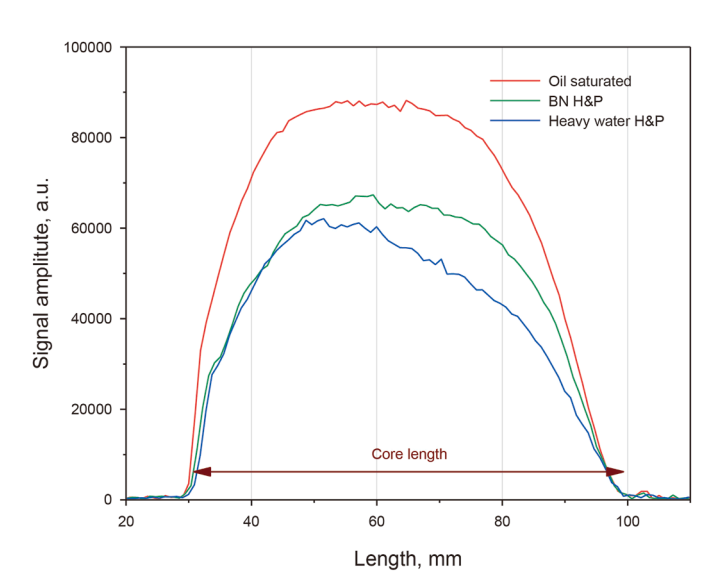


Fig. 10. Longitudinal T_2 signal comparison of different huff-n-puff agents in 5 \times 10⁻³ μ m² core samples.

and the puff pressure was 15 MPa. Injection pressure changes were monitored, and recovery efficiency was calculated using the weighting method after the experiment. Fig. 11 shows the recovery efficiency and soaking pressure changes under different core permeability conditions.

Fig. 11 shows that as permeability increased, the pressure change became larger. When permeability was below 1 \times $10^{-3}~\mu\text{m}^2$, the pressure change was negative, indicating that BN had better entry capability in low-permeability cores. This was mainly because lower-permeability cores had more micropores, where capillary forces were stronger. In higher-permeability cores, the capillary forces of nanoparticles weakened, while emulsification effects became more significant. This was likely the main reason for the pressure increase during soaking. The recovery efficiency, calculated by the weighting method, exceeded 50% in all cases. The highest recovery efficiency occurred in cores with a permeability of $1\times10^{-3}~\mu\text{m}^2$, suggesting optimal oil recovery efficiency near this permeability range. This may be due to a balance between capillary forces and emulsification effects at this pore scale.

Notably, similar to Table 3, the weighting method tended to overestimate recovery efficiency due to dead volume errors in saturation measurements. NMR T_2 signal analysis reduced this error. Therefore, to quantitatively analyze its recovery efficiency in pores of varying sizes, NMR T_2 analysis was employed. Fig. 12 shows the T_2 signals before and after huff-n-puff in low-permeability cores with different gas permeabilities.

Fig. 12 shows that after huff-n-puff, the T_2 signals in all low-permeability core samples decreased to varying degrees compared to before treatment. As the permeability decreased, the recovery efficiency of BN generally declined. During the initial oil-saturation stage of core samples, the T_2 signal intensity exhibited two distinct peak regions. The left peak represented oil content in micropores, while the right peak indicates oil in macropores. As the permeability increased, the oil content showed progressive growth in both macropores and micropores. Furthermore, both peaks shift rightward with increasing permeability, primarily due to changes in pore size distribution.

After BN huff-and-puff, recovery efficiency generally decreased with declining permeability. At permeabilities of 10×10^{-3} , 5×10^{-3} , 1×10^{-3} , 0.5×10^{-3} , and 0.1×10^{-3} μm^2 , the T_2 signal amplitudes demonstrated significant reduction. BN performed better

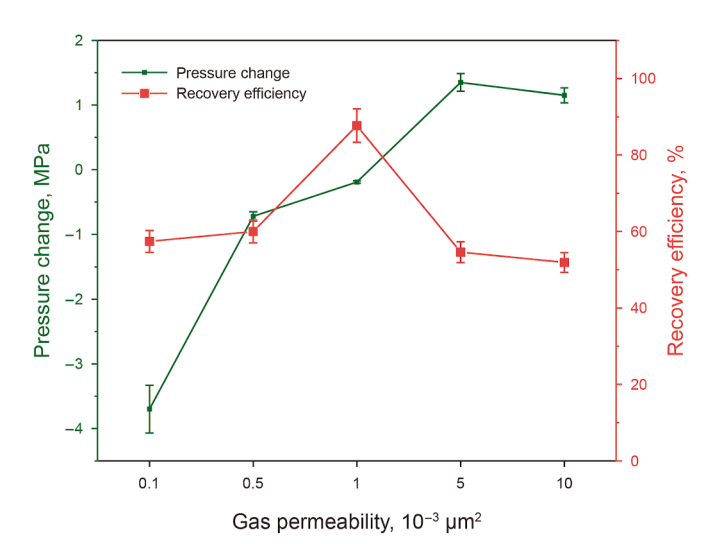


Fig. 11. Huff-n-puff performance of BN in low-permeability core samples with varying gas permeabilities.

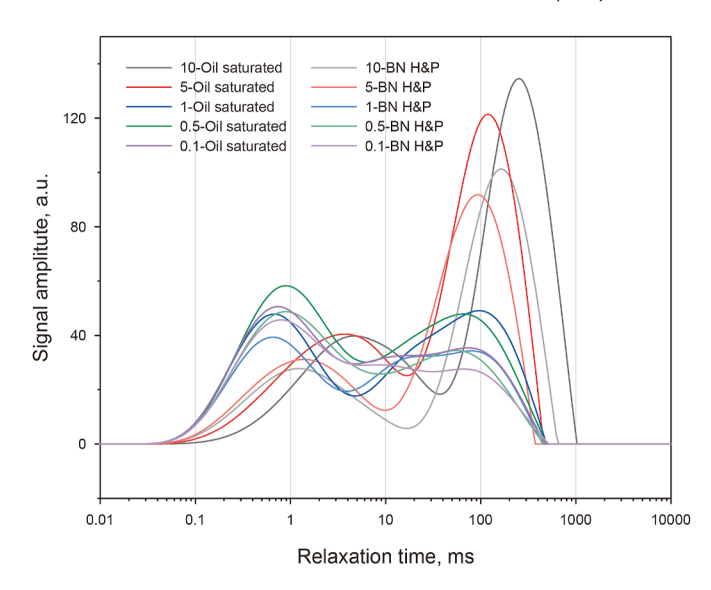


Fig. 12. T_2 signal comparison before and after BN huff-n-puff in core samples with varying gas permeabilities.

in $0.5 \times 10^{-3}~\mu\text{m}^2$ and above core samples compared to $0.1 \times 10^{-3}~\mu\text{m}^2$. This performance difference likely occurred because in $0.1 \times 10^{-3}~\mu\text{m}^2$ cores, micropores and nanopores dominated, and some BNs could not easily enter nanopores, reducing recovery efficiency. Notably, the increased signal intensity observed in micropores of some core samples resulted from crude oil being displaced from macropores into micropores under differential pressure and imbibition effects. However, the cumulative signal amplitude in micropores still showed an overall decrease.

To quantify the impact of pore size on recovery efficiency, the boundary between macropores and micropores was defined based on the valley of the NMR signal amplitude. The thresholds were set at 20, 10, 5, 5, and 5 ms for permeabilities of $10\times10^{-3},\,5\times10^{-3},\,1\times10^{-3},\,0.5\times10^{-3},\,\text{and}\,0.1\times10^{-3}\,\mu\text{m}^2,$ respectively. The recovery efficiencies in macropores and micropores for cores with different permeabilities are shown in Fig. 13.

Fig. 13 shows that the recovery efficiency in macropores

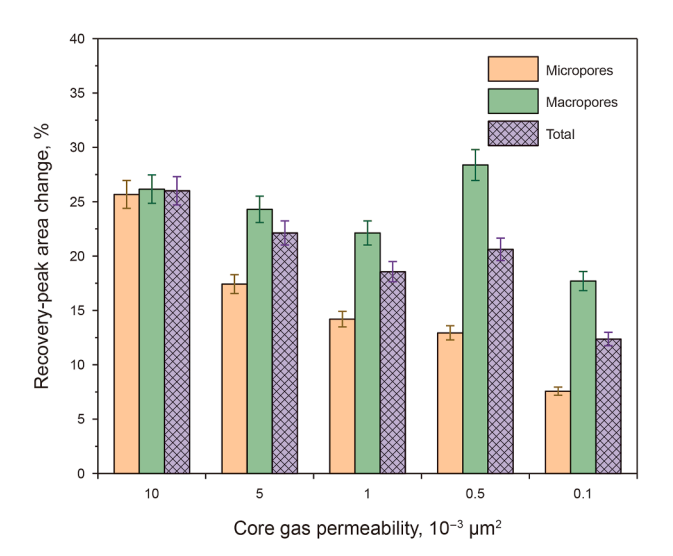


Fig. 13. T_2 signal peak area comparison of the first huff-n-puff cycle for BN in core samples with varying gas permeabilities.

generally decreased as the permeability declined. At core permeabilities of $10\times10^{-3},~5\times10^{-3},~1\times10^{-3},~0.5\times10^{-3},~\text{and}~0.1\times10^{-3}\,\mu\text{m}^2,$ the recovery efficiencies in macropores were 26.2%, 24.3%, 22.1%, 28.4%, and 17.7% OOIP, respectively. When the permeability decreased to $0.1\times10^{-3}\,\mu\text{m}^2,$ the recovery efficiency in macropores dropped significantly, decreasing by 10.7 percentage points compared to $0.5\times10^{-3}\,\mu\text{m}^2.$ This may be because, in $0.1\times10^{-3}\,\mu\text{m}^2$ core, the non-flowing liquid boundary layer occupied most of the flow space, reducing the effective flow cross-section. Additionally, due to size mismatch, some BN particles could not effectively enter nanopores to strip the adsorbed crude oil.

Furthermore, the recovery efficiency in micropores decreased more sharply with declining permeability than in macropores. Only at core permeability of $10\times 10^{-3}~\mu\text{m}^2$ did micropores exhibit a similar recovery efficiency to macropores. At core permeabilities of 10×10^{-3} , 5×10^{-3} , 1×10^{-3} , 0.5×10^{-3} , and $0.1\times 10^{-3}~\mu\text{m}^2$, the recovery efficiencies in micropores were 25.7%, 17.4%, 14.2%, 12.9%, and 7.6% OOIP, respectively. This indirectly indicated that the application of BN in low-permeability reservoirs was mainly constrained by micropores.

To observe pore activation along the core axis after huff-n-puff, NMR imaging analysis was used to obtain NMR images of BN in 10×10^{-3} and 5×10^{-3} µm² cores before and after BN huff-n-puff treatment, as shown in Fig. 14. Due to the small measurement volume of longitudinal units, the oil-saturated signal intensity in cores with permeability $\leq 1 \times 10^{-3}$ µm² was too weak. In imaging tests, system noise and minor hydrogen signals from the mineral matrix masked the oil signal, significantly reducing the signal-tonoise ratio. Thus, these results are not shown in this study.

Fig. 14 shows that after huff-n-puff, the grayscale intensity of the core images for low-permeability cores decreased significantly compared to the oil-saturated state. The grayscale reduction was more pronounced in the left side of the cores than in the right side for both 10×10^{-3} and $5\times10^{-3}~\mu\text{m}^2$ cores. This may be because rapid pressure release during the puff stage failed to support effective oil production from the right side. In actual oilfield applications, multiple huff-n-puff cycles or combined forward pressure-driven flooding may be required. The effect of cycle number on the BN huff-n-puff performance was investigated in Section 3.3.2.

Due to the low resolution of NMR imaging, the longitudinal T_2

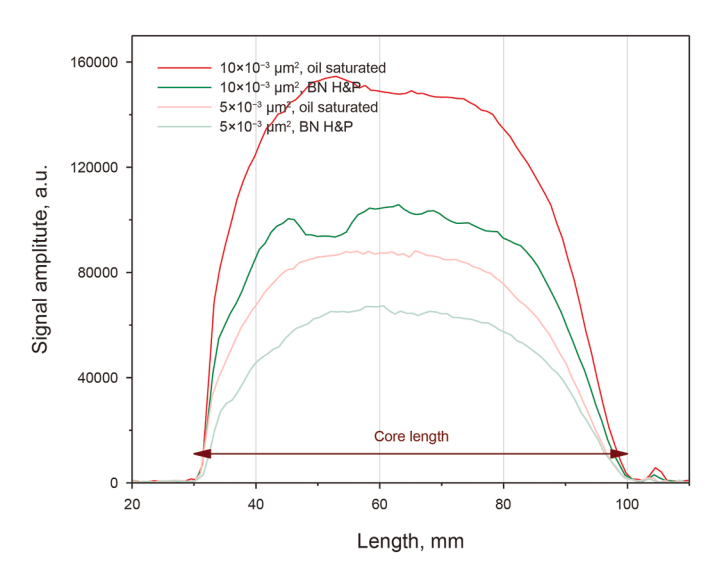


Fig. 15. Longitudinal T_2 signal comparison of BNs in low-permeability core samples with varying permeabilities.

signal projection method was also used to quantify axial pore activation during BN huff-n-puff. Fig. 15 presents the longitudinal T_2 signal changes before and after treatment in 10×10^{-3} and 5×10^{-3} µm² low-permeability cores.

Fig. 15 shows that after huff-n-puff, the signal amplitude reduction in the left side of the core samples was more significant than in the right side, which was consistent with the NMR imaging results. Specifically, the signal amplitude decreased more in the 30–60 mm segment (i.e., left 30 mm of the core) than in the 60–100 mm segment (i.e., right 40 mm of the core), but the difference was small. This indicates that the BN effectively swept the sandstone core within a length of 70 mm.

Additionally, this indirectly suggests that after anionic modification, the negative surface charge of the BN repelled the negative charge on the sandstone core surface, reducing adsorption. This significantly extended the effective working distance of the low-concentration BN solution in actual low-permeability sandstone reservoirs.

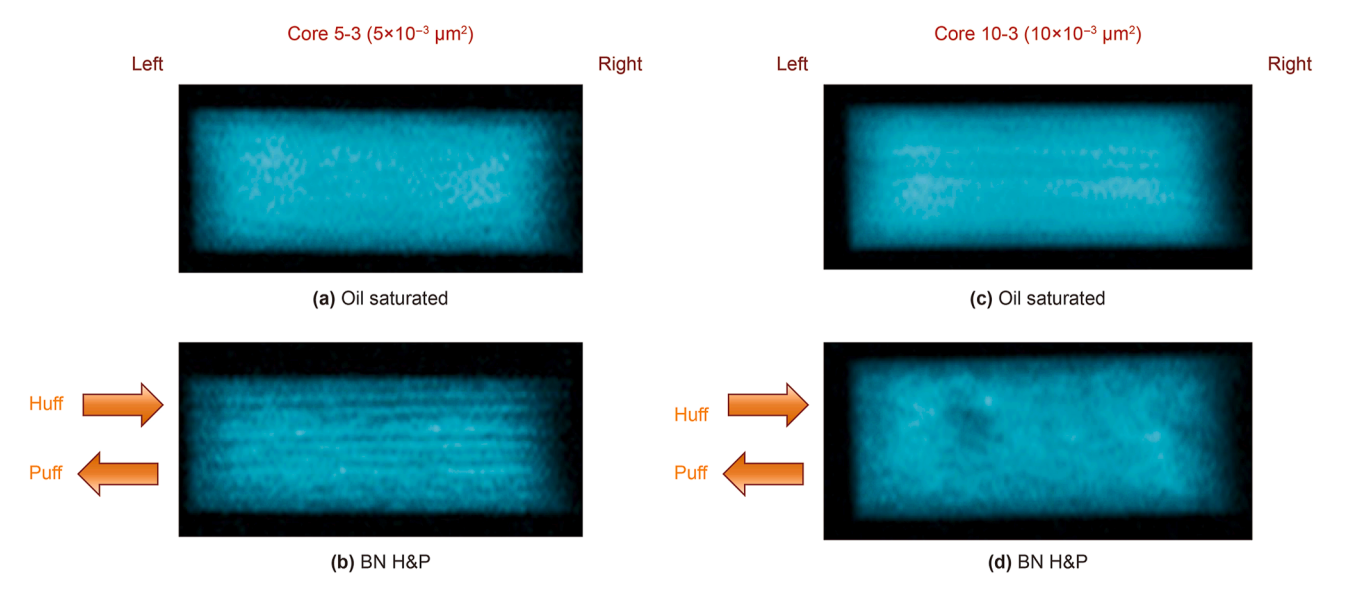


Fig. 14. NMR imaging comparison of BN huff-n-puff in core samples with varying permeabilities.

3.3.2. Multi-cycle huff-n-puff performance analysis

Fig. 7 has shown that after the first cycle of BN huff-n-puff, a large amount of remaining oil was still presented in the core samples based on the NMR signal. Since huff-n-puff operations typically used multi-cycle injection, we investigated the oil recovery performance under different huff-n-puff cycles. Due to the high uncertainty of core mass analysis for recovery calculations, NMR analysis was used to measure the signal amplitude of residual oil at different huff-n-puff stages. The results are shown in Fig. 16.

Fig. 16 shows that as the number of huff-n-puff cycles increased, the T_2 signal amplitude of the core decreased significantly, indicating more oil was recovered. The first two cycles showed the most notable changes: the signal peak of macropores decreased from 121.45 to 60.01 a.u., while the signal peak of micropores decreased from 40.45 to 33.97 a.u. Additionally, the micropore signal shifted slightly, possibly due to partial pore blockage by BNs or pore size reduction.

After the third cycle, the T_2 signal amplitude in both macropores and micropores decreased, but the reduction rate slowed. By the fourth cycle, the signal changes became minimal, with only the micropore signal still showing significant variation. To quantitatively evaluate the recovery efficiency in different pore types, the peak areas on the left and right sides of 10 ms in Fig. 16 were calculated to obtain the recovery efficiency changes based on NMR peak area, as shown in Fig. 17.

Fig. 17 shows that after multiple huff-n-puff cycles, the total recovery efficiency of BNs in the 5 \times $10^{-3}~\mu m^2$ core sample increased from 22.1% to 51.6% OOIP. The recovery efficiency increased significantly in the first three cycles, then stabilized during the fourth cycle, rising from 43.7% to 49.5% OOIP. This suggests that in actual oilfield applications, increasing the number of repeated fracturing or huff-n-puff operations could improve oil recovery. Therefore, numerical simulation can optimize the huffn-puff cycle design before oilfield implementation.

For oil mobilization in macropores and micropores, the first three cycles mainly mobilized oil from macropores, while the micropore oil recovery showed little change. From the fourth cycle, the increase in macropore recovery slowed, while micropore recovery increased significantly. This is because BNs had strong interfacial activity, meaning it had excellent automatic oil-seeking

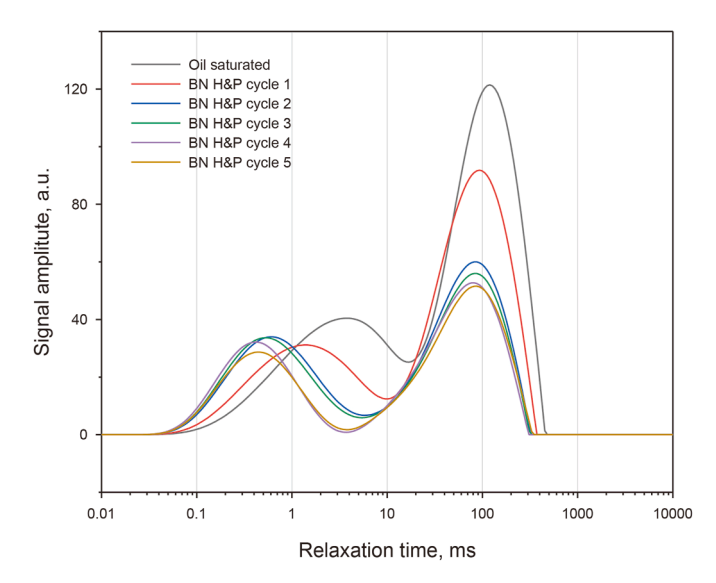


Fig. 16. T_2 signal comparison before and after multiple huff-n-puff cycles for BNs in $5\times 10^{-3}~\mu m^2$ core sample.

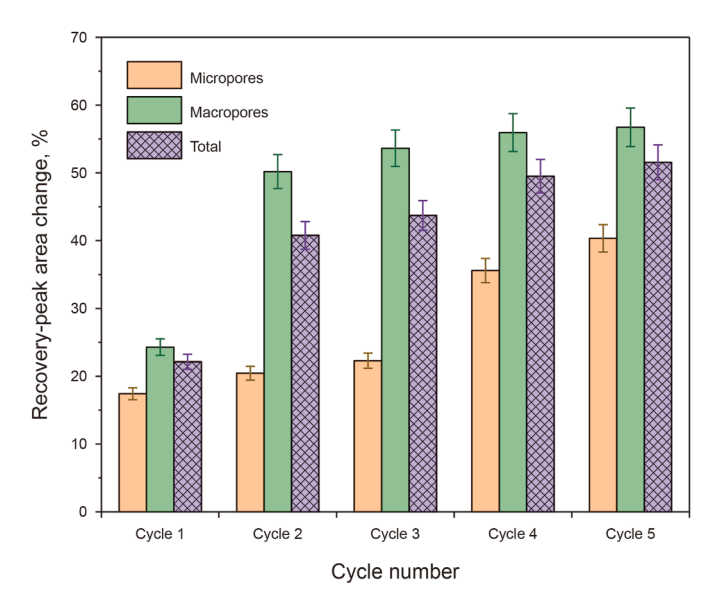


Fig. 17. Performance comparison of BN during multiple huff-n-puff cycles in $5\times 10^{-3}~\mu m^2$ core sample.

capability (Feng et al., 2022; Qu et al., 2022). After macropore oil was preferentially recovered, BNs could spontaneously enter micropores to displace oil.

Fig. 18 presents core NMR images during multi-cycle huff-npuff. The changes at the core inlet (left) showed that as the number of cycles increased, BNs penetrated deeper into the core. Additionally, it recovered more oil. To quantitatively analyze axial

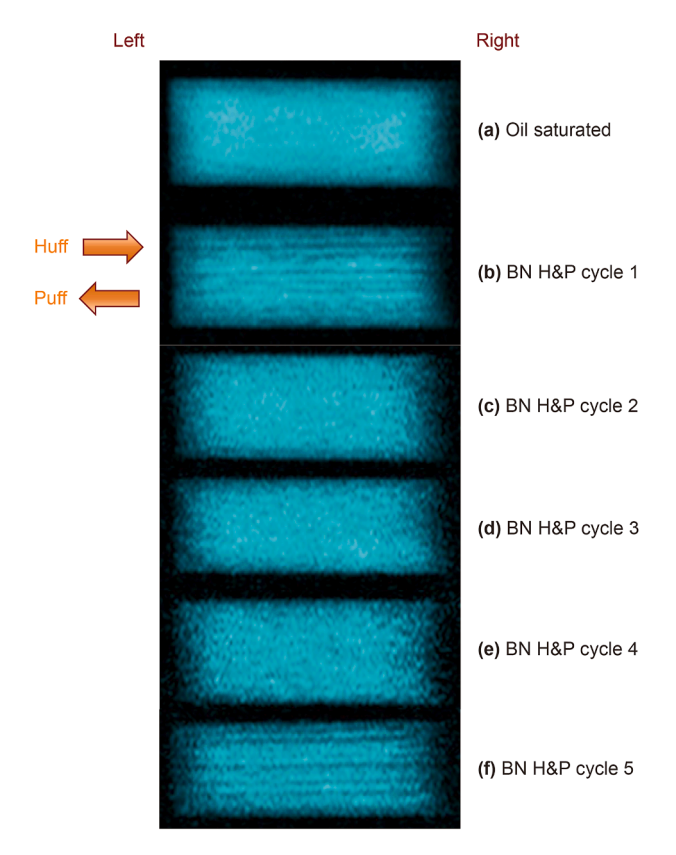


Fig. 18. NMR imaging comparison before and after multiple huff-n-puff cycles for BN in $5\times 10^{-3}~\mu m^2$ core sample.

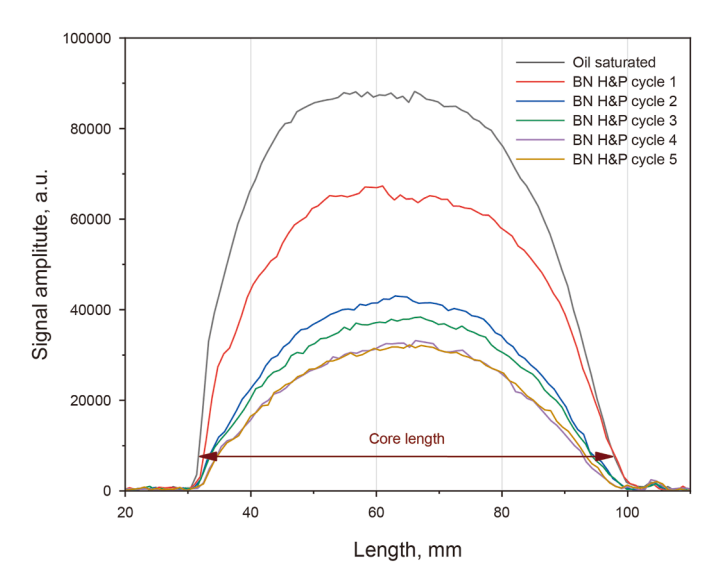


Fig. 19. Longitudinal T_2 signal comparison before and after multiple huff-n-puff cycles for BN in $5 \times 10^{-3} \ \mu m^2$ core sample.

signal amplitude changes, the longitudinal T_2 signal was also measured during multi-cycle huff-n-puff, as shown in Fig. 19.

The T_2 signal amplitude of the oil-saturated core was initially very high, with a peak value of 88,211 a.u. As the number of cycles increased, the T_2 signal amplitude decreased significantly. In addition, the inflection point length gradually extended, which aligned with the imaging results in Fig. 18. When the number of cycles exceeded 3, the signal amplitude decline slowed, but the recovery efficiency still increased slightly. After 4 cycles, the signal amplitude remained nearly constant, consistent with the T_2 signal amplitude changes in Fig. 16.

These results demonstrated that the huff-and-puff cycle number significantly impacted BNs' huff-n-puff performance. Particularly after the fourth cycle, when the oil saturation in macropores became relatively low (i.e., heavy water saturation increased), subsequent BN injection preferentially targeted oil remaining in micropores during the soaking period. This finding could provide important theoretical guidance for optimizing oilfield operation parameters in BN huff-and-puff processes. Furthermore, our study suggested that reservoir numerical simulation should be integrated with experimental results to optimize the cycle design when applying BN to reservoir stimulation.

In addition, these results also indicated that the longitudinal T_2 projection scanning method could quantitatively characterize the migration distance of the huff-n-puff agent along the injection direction. When combined with the conventional T_2 test data (pore size distribution) in Fig. 16, it could provide a clearer understanding of the mechanism of the huff-n-puff process.

4. Conclusions

This study investigated the huff-n-puff performance and adaptability of BNs in low-permeability core samples using NMR-assisted huff-n-puff experiments. TEM analysis, zeta potential measurements, crude oil emulsification tests, and contact angle measurements were used to analyze the interfacial properties of the BNs. NMR technology was applied to reveal the huff-n-puff mechanism at the microscopic level. The main conclusions were as follows.

- (1) After modification, BNs exhibited strong crude oil emulsification capability and interfacial activity, with nanoscale particle sizes.
- (2) Compared to injection water, BNs showed superior huff-n-puff performance. In the core sample with $5 \times 10^{-3} \ \mu\text{m}^2$ permeability, the recovery efficiency after the first cycle reached 22.1% OOIP (based on NMR peak area calculations).
- (3) NMR *T*² analysis provided microscale insights into the huffn-puff mechanism of BNs. The nanosheets preferentially entered micropores, recovering more oil.
- (4) NMR imaging combined with longitudinal *T*₂ signal projection analysis confirmed that the BNs entered micropores more efficiently and rapidly.
- (5) Compared to conventional weight-based calculation for oil recovery efficiency, NMR technology provided more accurate recovery efficiency results for low-permeability tight cores and explained the huff-n-puff mechanism at the microscopic level.
- (6) The BNs achieved high huff-n-puff recovery efficiency (12.37%–26.01% OOIP, based on NMR calculations) in low-permeability cores. In cores with permeability higher than $1 \times 10^{-3} \ \mu m^2$, the recovery efficiency reached ~20% OOIP.
- (7) The number of huff-n-puff cycles significantly affected the performance of BNs, with the optimal cycle number being 4. When the cycle number increased from 3 to 4, the "automatic oil-seeking" capability of BNs in micropores became more pronounced.
- (8) This study primarily used artificial sandstone cores for mechanistic analysis. For oilfield applications, natural core samples should be tested for adaptability, and numerical simulations should be conducted to optimize the huff-npuff cycle number.

CRediT authorship contribution statement

Si Guo: Writing – original draft, Validation, Investigation, Data curation. **Hong-Bin Cheng:** Validation, Investigation, Data curation. **Hong-Gen Tan:** Validation, Investigation, Data curation. **Hong-Yu Li:** Investigation, Data curation. **Jiong Zhang:** Investigation, Data curation. **Ying-Qi Gao:** Investigation, Data curation. **Dao-Yi Zhu:** Writing – review & editing, Writing – original draft, Validation, Supervision.

Declaration of competing interest

The authors declare that they have no known competing financial interests or personal relationships that could have appeared to influence the work reported in this paper.

References

- Al-Muntasheri, G.A., Liang, F., Hull, K.L., 2017. Nanoparticle-enhanced hydraulic-fracturing fluids: A review. SPE Prod. Oper. 32 (2), 186–195. https://doi.org/10.2118/185161-PA.
- Almahfood, M., Bai, B., 2018. The synergistic effects of nanoparticle-surfactant nanofluids in EOR applications. J. Petrol. Sci. Eng. 171, 196–210. https://doi. org/10.1016/j.petrol.2018.07.030.
- Bai, H., Zhou, F., Zan, J., Zhang, M., Xu, H., Lang, H., Zhu, L., Zou, Y., Liu, Z., Yao, E., 2023. Stimulation mechanism and model establishment of enhanced imbibition oil recovery for a nano fracturing fluid. J. Petrol. Sci. Eng. 220, 111189. https://doi.org/10.1016/j.petrol.2022.111189.
- Davoodi, S., Al-Shargabi, M., Wood, D.A., Rukavishnikov, V.S., Minaev, K.M., 2022. Experimental and field applications of nanotechnology for enhanced oil recovery purposes: A review. Fuel 324, 124669. https://doi.org/10.1016/j.fuel.2022.124669.
- Fan, H., Liu, X., Li, G., Li, X., Radwan, A., Yin, S., 2024. Study on characteristics, efficiency, and variations of water flooding in different stages for low permeability oil sandstone. Energy Sci. Eng. 12 (11), 5245–5265. https://doi.org/

10.1002/ese3.1942.

- Fan, Q., Luo, M., Bai, Y., Wang, K., Pu, C., Zhan, Y., 2024. Experimental and numerical simulation study on enhanced oil recovery by N₂-assisted water huff-n-puff in a tight oil reservoir. Geoenergy Sci. Eng. 241, 213133. https://doi.org/10.1016/j. geoen_2024_213133.
- Feng, Y., Hou, J., Yang, Y., Wang, D., Wang, L., Cheng, T., Liu, Y., 2022. Molecular dynamics simulation research on microscopic mechanism of two-dimension (2-D) black nanosheet at water/oil interface. Oilfield Chem. 39 (2), 311–317. https://doi.org/10.19346/j.cnki.1000-4092.2022.02.021 (in Chinese).
- Geng, X., Ding, B., Guan, B., Sun, H., Zan, J., Qu, M., Liang, T., Li, H., Hu, S., 2024. New insight of nanosheet enhanced oil recovery modeling: Structural disjoining pressure and profile control technique simulation. Energies 17 (23), 5897. https://doi.org/10.3390/en17235897.
- He, D., Huang, T., Mao, J., Li, D., Sun, Y., 2024. Research and application of fracturing huff and puff technology in low permeability reservoirs. In: SPE Asia Pacific Oil and Gas Conference and Exhibition. https://doi.org/10.2118/221308-MS.
- Mo, C., Zhang, G., Tang, Y., Chen, Z., Zeng, D., Li, H., Tang, L., Yin, X., 2024. Characterizing residual oil distribution in heavy oil reservoirs after multiple hot water huff and puff: A comprehensive analysis. Energy & Fuels 38 (4), 2866–2873. https://doi.org/10.1021/acs.energyfuels.3c04547.
- Qin, Z., He, Y., Wang, N., Zhao, N., Yao, Z., Wu, L., Ding, Y., Tang, S., Liu, X., 2024. Improved relative permeability models incorporating water film effects in low and ultra-low permeability reservoirs. Energy & Fuels 38 (17), 16218–16239. https://doi.org/10.1021/acs.energyfuels.4c02096.
- https://doi.org/10.1021/acs.energyfuels.4c02096.
 Qu, M., Hou, J., Liang, T., Qi, P., 2021. Amphiphilic rhamnolipid molybdenum disulfide nanosheets for oil recovery. ACS Appl. Nano Mater. 4 (3), 2963–2972. https://doi.org/10.1021/acsanm.1c00102.
- Qu, M., Liang, T., Hou, J., Liu, Z., Yang, E., Liu, X., 2022. Laboratory study and field application of amphiphilic molybdenum disulfide nanosheets for enhanced oil recovery. J. Petrol. Sci. Eng. 208, 109695. https://doi.org/10.1016/j. petrol.2021.109695.
- Quintero, H., Mattucci, M., Hawkes, R., Zhang, K., O'Neil, B., 2018. Nano-particle surfactant in hydraulic fracturing fluids for enhanced post frac oil recovery. In: SPE Canada Unconventional Resources Conference. https://doi.org/10.2118/ 189780-MS
- Raj, I., Qu, M., Xiao, L., Hou, J., Li, Y., Liang, T., Yang, T., Zhao, M., 2019. Ultralow concentration of molybdenum disulfide nanosheets for enhanced oil recovery. Fuel 251, 514–522. https://doi.org/10.1016/j.fuel.2019.04.078.
- Wang, P., Hu, Y., Zhang, L., Meng, Y., Ma, Z., Wang, T., Zhang, Z., Fang, J., Liu, X., You, Q., Zhang, Y., 2024. Experimental study of the influencing factors and mechanisms of the pressure-reduction and augmented injection effect by nanoparticles in ultra-low permeability reservoirs. Pet. Sci. 21 (3), 1915–1927. https://doi.org/10.1016/j.petsci.2023.11.024.
- Wang, Q., Zhou, F., Su, H., Zhang, S., Dong, R., Yang, D., Wang, Y., Chen, Z., Li, J., 2024. Experimental evaluations of nano high-viscosity friction reducers to improve acid fracturing efficiency in low-permeability carbonate reservoirs. Chem Eng J. 483, 149358. https://doi.org/10.1016/j.cej.2024.149358.
- Wu, H., Chang, J., Xu, G., Shao, W., Li, G., Hou, J., 2024. In-situ emulsification and viscosification system of surfactant-assisted Janus nanofluid and its profile control effect. Adv. Geo-Energy Res. 14 (2), 135–146. https://doi.org/10.46690/ ager.2024.11.06.
- Xu, H., Li, Y., Yu, G., Yang, S., Li, B., Zhou, F., Yao, E., Bai, H., Liu, Z., 2023. The enhancement of performance and imbibition effect of slickwater-based

- fracturing fluid by using MoS₂ nanosheets. Pet. Sci. 20 (4), 2187–2201. https://doi.org/10.1016/j.petsci.2022.12.008.
- Xu, Z., Zhao, M., Xie, Y., Li, T., Meng, X., Dong, Y., Yang, Z., Dai, C., 2024. Nano-slickwater fracturing fluid with enhanced imbibition capacity for low-permeability reservoirs. Energy & Fuels 39 (2), 1141–1151. https://doi.org/10.1021/acs.energyfuels.4c04890.
- Yekeen, N., Padmanabhan, E., Idris, A.K., Chauhan, P.S., 2019. Nanoparticles applications for hydraulic fracturing of unconventional reservoirs: A comprehensive review of recent advances and prospects. J. Petrol. Sci. Eng. 178, 41–73. https://doi.org/10.1016/j.petrol.2019.02.067.
- Zhang, T., Dai, C., Wang, K., Li, Z., Gao, M., Adenutsi, C.D., Zhao, M., 2024. Analysis of spontaneous and dynamic imbibition characteristics of silica-based nanofluid in microscopic pore structure of tight oil reservoirs. Langmuir 40 (47), 25250–25261. https://doi.org/10.1021/acs.langmuir.4c03577.
- 25250–25261. https://doi.org/10.1021/acs.langmuir.4c03577.

 Zhao, J., Peng, M., Qi, X., Wen, Q., Yang, J., 2024. Low-carbon and high-efficiency nanosheet-enhanced CO₂ huff-n-puff (HnP) for heavy oil recovery. Chemical Engineering Journal 500, 156875. https://doi.org/10.1016/j.cej.2024.156875.
- Zhou, B., You, Q., Li, Y., Chu, Z., Zhang, L., Wang, P., Liu, C., Dai, C., 2022. Preparation and performance evaluation of an active nanofluid for enhanced oil recovery in ultra-low permeability reservoirs. J. Mol. Liq. 347, 118331. https://doi.org/ 10.1016/j.molliq.2021.118331.
- Zhou, M., Yang, X., Gao, Z., Wu, X., Li, L., Guo, X., Yang, Y., 2022. Preparation and performance evaluation of nanoparticle modified clean fracturing fluid. Colloids Surf. A Physicochem. Eng. Asp. 636, 128117. https://doi.org/10.1016/j.colsurfa.2021.128117.
- Zhu, D.Y., Zhao, Y.H., Zhang, H.J., Zhao, Q., Shi, C.Y., Qin, J.H., Su, Z.H., Wang, G.Q., Hou, J.R., 2023. Combined imbibition system with black nanosheet and low-salinity water for improving oil recovery in tight sandstone reservoirs. Pet. Sci. 20 (3), 1562–1571. https://doi.org/10.1016/j.petsci.2022.12.004.Zhu, D., Gao, Y., Bai, L., Guo, S., 2024a. Development of anionic-modified black
- Zhu, D., Gao, Y., Bai, L., Guo, S., 2024a. Development of anionic-modified black nanosheet and its oil imbibition performance in ultralow-permeability reservoirs. Energy & Fuels 38 (15), 14149–14157. https://doi.org/10.1021/acs. energyfuels.4c02952.
- Zhu, D., Li, B., Chen, L., Zhang, C., Zheng, L., Chen, W., Li, Z., 2024b. Experimental investigation of CO₂ foam flooding-enhanced oil recovery in fractured lowpermeability reservoirs: Core-scale to pore-scale. Fuel 362, 130792. https:// doi.org/10.1016/j.fuel.2023.130792.
- Zhu, D., Qin, J., Gao, Y., Zhang, J., Guo, S., Liu, S., Zhao, J., Gao, Y., 2024c. Dispersion stability and oil displacement effect of modified black nanosheet. Energy & Fuels 38 (13), 11635–11643. https://doi.org/10.1021/acs.energyfuels.4c02155.
- Zhu, D., Guo, S., Lu, J., Yang, Y., Zhang, T., Zhang, J., Gao, Y., Tan, H., Cheng, H., Li, H., 2025. Influence of injection parameters of black nanosheets on enhancing oil recovery performance in low-permeability reservoirs. Energy & Fuels 39 (13), 6241–6250. https://doi.org/10.1021/acs.energyfuels.5c00546.
- Zhu, J., Tang, X., Li, X., Wen, Y., Deng, Z., Rao, D., Yang, Z., Liu, C., 2024. The reservoir injury rules of water injection to an ultralow permeability reservoir: Experimental research based on core-NMR and microfluidic technology. Energy & Fuels 38 (16), 15131–15146. https://doi.org/10.1021/acs.energyfuels.4c01797.
- Zuo, M.S., Chen, H., Liu, X., Liu, H., Wu, Y., Qi, X., 2024. Fractal model of spontaneous imbibition in low-permeability reservoirs coupled with heterogeneity of pore seepage channels and threshold pressure. Pet. Sci. 21 (2), 1002–1017. https://doi.org/10.1016/j.petsci.2023.10.027.